

In-flight main beam reconstruction for Planck-LFI

C. Burigana¹, P. Natoli², N. Vittorio², N. Mandolesi¹, and M. Bersanelli³

¹ Istituto TeSRE/CNR, via P. Gobetti 101, I-40122 Bologna, Italy

² Dipartimento di Fisica, Università di Roma “Tor Vergata”, via della Ricerca Scientifica 1, I-00133, Roma, Italy

³ Dipartimento di Fisica, Università di Milano, and IFC/CNR, via Celoria 16, I-20133, Milano, Italy

Submitted on A&A, 02.11.2000

Abstract. In-flight measurement of the antenna main beams of the PLANCK instruments is a crucial input to the data analysis pipeline. We study the main beam reconstruction achievable through external planets using a flight simulator to model their observation. We restrict our analysis to the 30 GHz LFI channel but the method can be easily extended to higher frequency channels. We show that it is possible to fit the antenna response from Jupiter and Saturn to obtain an accurate, robust, simple and fast reconstruction of the main beam properties under very general conditions, independently of the calibration accuracy. In addition, we find that a bivariate Gaussian approximation of the main beam shapes represents a significant improvement with respect to a symmetric representation. We also show that it is possible to combine the detection of the planet’s transit and Planck’s very accurate in-flight calibration to measure the planet’s temperature at millimetric wavelengths with an accuracy at the % level. This work is based on PLANCK-LFI activities.

Key words: *Cosmology: cosmic microwave background – Space vehicles – Telescopes – Methods: data analysis – Solar System: general*

1. Introduction

The PLANCK Surveyor¹ is the ESA space mission devoted to the study of the Cosmic Microwave Background. PLANCK will have an impact on a number of scientific issues, such as the physics of the early universe, structure formation theory and cosmological parameters determination (Bersanelli et al. 1996). In order to reach the necessary level of sensitivity it is important to understand systematics and to keep them under control. In this paper we will focus on the behavior of the PLANCK Low Frequency Instrument (LFI, Mandolesi et al. 1998) antenna patterns. For simplicity, we will restrict our analysis to the 30 GHz LFI channel but the method we present here can be easily extended to higher frequency channels.

Send offprint requests to: burigana@tesre.bo.cnr.it

¹ <http://astro.estec.esa.nl/SA-general/Projects/Planck/>

The beam pattern is affected by optical distortions, which depend on the telescope design and on the arrangement of the various feed horns in the focal plane. These effects degrade both angular resolution and sensitivity (e.g., Mandolesi et al. 2000a,b). Therefore, accurate measurement of the beam pattern is a crucial input to the data analysis pipeline.

Due to their small angular size external planets produce large signals only when seen in the main beam. As such, they represent a unique possibility to recover directly from the data the in-flight behavior of the main beam. This point was already addressed, in the framework of the PLANCK mission, by Bersanelli et al. 1997 for the simple case of a Gaussian symmetric antenna response. We extend here this analysis to quantify our ability to reconstruct a more realistic, asymmetric beam pattern.

The plan of this paper is as follows. In Sect. 2 we describe our main tools and assumptions. In Sect. 3 we discuss the quality of the main beam reconstruction and the implications for the treatment of PLANCK data. As a byproduct of our simulations, we also verify in Sect. 4 the validity of the PLANCK optical design to strongly suppress straylight contamination from internal Solar System bodies. In Sect. 5 we summarize our findings and draw our conclusions.

2. Method

In order to attack the problem of the in-flight main beam reconstruction, we have to: (i) describe the PLANCK orbit and scanning strategy; (ii) quantify the antenna response; (iii) exploit the planet’s mm emission and positions; (iv) simulate the PLANCK observations of the external planets (basically Jupiter and Saturn). Here we briefly discuss these points separately.

2.1. PLANCK orbit and scanning strategy

The selected orbit for the PLANCK satellite is a Lissajous orbit around the Lagrangian point L2 of the Sun-Earth system (e.g., Bersanelli et al. 1996). In the nominal operation scheme the spacecraft spins at 1 r.p.m. around an

axis kept parallel to the ecliptic plane. Every hour the spin axis is moved by $2.5'$ maintaining its anti-solar direction. The telescope optical axis is at an angle α from the spin axis direction. The spin axis might precede about the anti-solar direction, with a period of about six months and an amplitude of about 10° . This spacecraft movement is of course over imposed to the Lissajous orbit and to the spin axis hourly shift. In this paper we consider values of α between 80° and 90° , i.e. about the value of 85° recently recommended by the PLANCK Science Team. We make use of the PLANCK flight simulator described in detail by Burigana et al. 1997, 1998 and Maino et al. 1999 properly modified to model the PLANCK observations of the Solar System bodies and the spacecraft motion (see, e.g., Bersanelli et al. 1997).

For what follows, it is convenient to introduce a telescope “reference frame” (hereafter rf) $\{x_T, y_T, z_T\}$ with the z_T axis coincident with the direction of the telescope line of sight (the \hat{p} direction, say) and with the $x_T - y_T$ plane identifying the telescope field of view plane (we choose to orient \hat{x}_T towards the intersection of the $x_T - y_T$ plane with the spin axis \hat{s} or, in the case $\alpha = 90^\circ$, $\hat{x}_T \parallel \hat{s}$). For the considered scanning strategies the spin axis and the telescope directions (\hat{s} and \hat{p} , respectively) are easily derived given the observation time, the spinning frequency and the boresight angle α . So it is always possible to pass from a chosen celestial rf to the telescope rf (and viceversa) by a suitable Eulerian rotation of the considered rf.

2.2. Antenna angular pattern

The PLANCK High Frequency Instrument (HFI, Puget et al. 1998) is located at the center of the focal plane. The LFI feed horns surround HFI and are then substantially off-axis. For instance, with a telescope of 1.5 m class, the 30 GHz beams are at about $\simeq 5^\circ$ from \hat{p} . So, it is convenient to define a beam rf $\{x_b, y_b, z_b\}$ with the z_b axis coincident with beam axis \hat{b} and with the $x_b - y_b$ plane slightly tilted with respect to the telescope field of view plane (we keep the convention of obtaining the beam rf from the telescope rf through a rotation of the telescope rf about an axis horthogonal to the plane identified by \hat{p} and \hat{b} by the angle necessary to transport \hat{p} to \hat{b}).

As we know the position of each feed horn in the focal plane, we can always pass from the telescope rf to the beam rf and viceversa. In fact, the flight simulator determines for every time step the orientations in the sky of the telescope and beam reference frames, to compute the antenna response for a given line of sight.

2.2.1. Main beam

Recent improvements on the PLANCK optical design based on aplanatic solutions (Mandolesi et al. 2000b) show that the main beams are roughly elliptical, with an ellipticity ratio $r \lesssim 1.4$ (Alcatel, private reference, PL-AS-TN-

022). Therefore, we approximate the antenna pattern as an off-axis bivariate Gaussian beam. For simplicity, we will consider the bivariate Gaussian beam projected onto the field of view plane (i.e. we will consider this beam representation on the $x_T - y_T$ plane, and not on the $x_b - y_b$ beam plane). To be accurate one has to say that if the true beam shape is elliptical in the $x_b - y_b$ plane, it gets distorted by the projection on the $x_T - y_T$ plane. However, since the off-axis angle even for the 30 GHz beam is small, this distortion is negligible and, if anything, does not change the elliptical nature of the beam response. In addition, a realistic main beam distortion implies a deviation from the elliptical shape larger than that introduced by this projection. So, let (x_T^*, y_T^*) identify the projection of the beam centre unit vector onto the $x_T - y_T$ plane. Let ϵ be the angle between the x_T -axis and the principal axis of the bivariate Gaussian. The (normalized to the maximum) beam response can be then expressed as:

$$J = \exp\left[-\frac{1}{2} (\mathcal{R}\mathbf{u})^t \Sigma^{-1} \mathcal{R}\mathbf{u}\right] \quad (1)$$

where

$$\mathbf{u} = \begin{pmatrix} x_T - x_T^* \\ y_T - y_T^* \end{pmatrix},$$

$\Sigma = \text{diag}(\sigma_+^2, \sigma_-^2)$ contains the bivariate’s beam dispersions along the ellipse principal axis and \mathcal{R} is the rotation matrix for an angle ϵ in the $x_T - y_T$ plane:

$$\mathcal{R} = \begin{pmatrix} \cos \epsilon & \sin \epsilon \\ -\sin \epsilon & \cos \epsilon \end{pmatrix}.$$

It is then convenient to define the beam “sigma” $\sigma = \sqrt{\sigma_+ \sigma_-}$ and the ellipticity ratio $r = \sigma_+ / \sigma_-$.

2.2.2. Far side lobes

A realistic description of the antenna far side lobes has to rest on the accurate optical calculations of de Maagt et al. 1998 for the PLANCK telescope including shields. Several cuts at constant azimuthal angle ϕ are shown in Fig. 1 as a function of the colatitude angle θ from the beam axis \hat{b} . In the “antispillover” region [about $(\theta, \phi) \sim (90^\circ, 180^\circ)$] where it is mostly important to evaluate the effects of straylight from the internal bodies of the Solar System (i.e. Sun, Earth and Moon) the pattern response drops down to approximately $\sim 100\text{dB}$. At such a level of rejection, according to the PLANCK requirements, one expects that Sun, Earth and Moon are completely harmless for the mission. We will further discuss this point in Sect. 4.

2.3. Planet’s mm emissions and positions

2.3.1. External Planets

Several authors reported measurements of the planets brightness temperature at millimeter wavelengths with

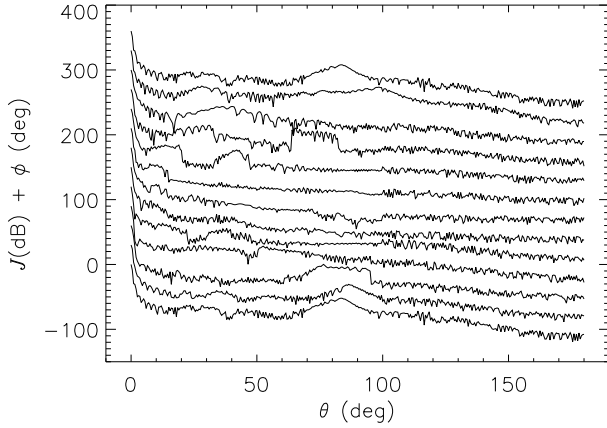


Fig. 1. Several cuts of the full antenna pattern, in dB, as computed by de Maagt et al. 1998. The lines refer to the antenna response for θ between 0° and 180° and, from the bottom to the top, with ϕ at steps of 30° from 0° to 360° (each cut is vertically shifted for graphic purposes to have the value at the point at $\theta = 0^\circ$ equal to the considered value of ϕ).

typical uncertainties of $3 \div 5\%$ (see, e.g., Bersanelli et al. 1997 and references therein). The quite large uncertainties associated with these values prevents one from using planets for accurate temperature calibration of the PLANCK time order data. This will be done, to better than a 1%, by using the diffuse signature of the CMB dipole anisotropy (Bersanelli et al. 1997). However, for the purpose of beam reconstruction it is not necessary to have a detailed knowledge of the planet emission. It only matters that the source is stable and sufficiently bright to be detectable even when the source is far from the beam axis. This requirement is crucial to sample the antenna beam response at different angles. For this reason we will consider here only Jupiter and Saturn, which are the brightest of the external planets. On the basis of the published data, we will assume hereafter that Jupiter and Saturn have, at 30 GHz, brightness temperatures of $T_{jup}^{(b)} = 152$ K and $T_{sat}^{(b)} = 133$ K, respectively.

2.3.2. Inner bodies of the Solar System

The amount of straylight contaminations from the inner bodies of the Solar System can be easily quantified. We restrict ourselves to the Sun, Earth and Moon, because of their high intrinsic temperatures and because of the solid angles subtended from L2. We will use $T_{sun}^{(th)} = 6000$ K, $T_{earth}^{(th)} = 300$ K and $T_{moon}^{(th)} = 250$ K as the temperatures associated with the millimetric thermal emission of Sun, Earth and Moon, respectively.

2.4. PLANCK observations of the external planets

We use the PLANCK flight simulator in order to model the transit of the planets in the PLANCK field of view. In particular, Jupiter and Saturn will be observed twice in about a year. The solid angle of the external planets as seen by PLANCK is very small compared to the beam size. Thus, the PLANCK observations of the Jupiter (Saturn) will yield

$$T_{30GHz}[\hat{\gamma}(t)] \simeq \frac{T^{(b)}\pi(R/d)^2 J[\hat{\gamma}(t) - \hat{b}]}{\int_{4\pi} J(\hat{\gamma}) d\Omega}. \quad (2)$$

In this equation T_{30GHz} is the observed Jupiter (Saturn) brightness temperatures @ 30 GHz; $T^{(b)}$, R and d represent the intrinsic Jupiter (Saturn) brightness temperature, radius and distance, respectively; J is the antenna response and $\hat{\gamma}(t)$ identifies the angular position of the planet as seen by PLANCK, the time dependence being fixed by the scanning strategy.

3. In-flight recovery of the main beam pattern

The PLANCK Time Ordered Data (TOD) are affected by instrumental noise. Therefore, our capability to recover the main beam pattern rests on the possibility to clearly detect a bright source (e.g., Jupiter), even when significantly far from the beam axis. A proper description of the PLANCK-LFI instrumental noise should in principle include a $1/f$ contribution (see, e.g., Bersanelli et al. 1996, Seiffert et al. 1997). The knee-frequency of the $1/f$ noise is expected to be comparable with the spinning frequency. However, it has been shown that destriping algorithms can very efficiently remove this low frequency noise component even under more pessimistic conditions (see, e.g., Maino et al. 1999 and references therein) and return a TOD that we will assume, accordingly with the goals of this paper, white noise dominated. So, in what follows we will model the TOD noise component as pure white noise, with the PLANCK goal sensitivities discussed by Bersanelli et al. 1999 (private reference, PLANCK Low Frequency Instrument, Instrument Science Verification Review, October 1999, LFI Design Report). In principle, the signal fluctuations introduced by CMB and foreground anisotropies behave as a noise source in this context. However, since they can be accurately subtracted from the TOD by using the PLANCK final maps, we neglect them in what follows. We adopt here a simple scanning strategy with $\alpha = 90^\circ$. In the simulations presented in Sect. 3.1, we oversample each scan circle every $\simeq 5'$ (i.e. roughly 6 points per FWHM @ 30GHz) and shift the spin axis by $5'$ every two hours. After simulating the Jupiter and Saturn transits we extract from the time ordered scans a few (~ 100) chunks comprising the source transit. Since the source is pointlike, these chunks give, when displayed one after the other and having taken into account the small variations of planet

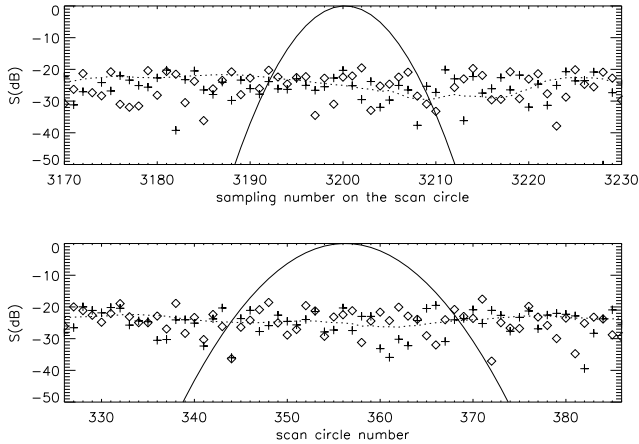


Fig. 2. Top panel: signals of different components along the scan circle with the maximum of Jupiter contribution during its first transit. Solid line: Jupiter signal; crosses: white noise; diamonds: $1/f$ noise coupled to white noise; dotted line: signal from CMB and extragalactic source fluctuations and Galaxy emission modelled according to Burigana et al. 2000a and references therein. Bottom panel: the same as in the top panel, but considering the signal at the same scan position, where Jupiter signal is maximum, for different scan circles. According to the simulation parameters, by multiplying the scan circle number or the sampling number on the scan circle by 5 we have respectively the angular displacement between different scan circles and (approximately, owing to the off-axis beam position) the angular displacement between different samplings along the scan circle, expressed in arcmin. We consider here the case of an elliptical beam with $r = 1.3$, clearly visible in the different spread of Jupiter signal in the two panels. Note that the signal to noise ratio is larger than unit up to $-(20 \div 25)$ dB, i.e. at about $(3 \div 3.5)\sigma$. [Signals in dB normalized to the maximum Jupiter signal at its first transit].

distance in the different samplings, a 2-D plot of the beam profile, $\simeq 8.3^\circ \times 8.3^\circ$ wide.

In Fig. 2 we show the expected signal from Jupiter as seen along the scan circle which crosses the source at the maximum (top panel) and as seen along an arc orthogonal to this circle (bottom panel). The signal to noise can be improved, wrt the case of a single receiver and transit, by considering that two LFI receivers are coupled to the same optical beam, that there are two 30 GHz beams with the same optical properties and that two (three) transits of both Jupiter and Saturn are expected for a one year (for a $14 \div 15$ months) mission. This obviously increases the signal to noise ratio by a factor of $2\sqrt{2}$ ($2\sqrt{3}$). As a result, @ 30 GHz, the shape of the main beam can be recovered down to $-(25 \div 32.5)$ dB, i.e. at about $(3.5 \div 4)\sigma$.

3.1. Recovery of the main beam parameters

We consider both a symmetric and an elliptical beam, with ellipticity ratio $r = 1.3$. The numerical values of the beam parameters are shown in Table 1. We use Eq.(1) to model the antenna response. We fit the beam shape theoretical parameters to the 2D plot of the beam response obtained as mentioned at the end of the previous section.

The results of the fits are shown in Table 2. We fit also an additional parameter, r_k , related to the planet brightness temperature and to the average distance of the planet from the spacecraft, $\langle d \rangle$, for the points considered in the fit: $r_k = \pi(R/\langle d \rangle)^2 T^{(b)} / \int_{4\pi} J(\hat{\gamma}) d\Omega$. We recover the full set of parameters with very high accuracy (Burigana et al. 2000c), the χ^2/DOF being always very close (to better than 1%) to the unity value. It is obviously more efficient to recover the beam pattern parameters using Jupiter rather than Saturn, simply because Jupiter is brighter.

An interesting byproduct of the beam fitting procedure is the possibility of estimating the planet's antenna temperature, or more properly the product $T^{(b)}R^2$ relevant for the planet's emission at the considered frequency. This quantity, as previously stated, is a poorly known quantity at LFI's frequencies. By considering Eq. (1) it is clear that the latter temperature, $T^{(b)}$ is related to the normalization of the bivariate which is in turn very well constrained by our fit. The ability to estimate $T^{(b)}$ then rests upon the overall calibration accuracy² and on the knowledge of the total antenna beam integral. Calibration for PLANCK will be provided by continuous observation of the CMB dipole signature and its modulation introduced by the spacecraft motion (Bersanelli et al. 1997) and is expected to be accurate to within 1%. The total integral of the antenna pattern poses a more serious problem, as the contribution of the far side lobes goes undetected when using a celestial source. However, optical calculations (de Maagt 1998) show that the contribution to the antenna pattern coming from outside the main lobe is expected to be $< (2 \div 3)\%$ of the total. The uncertainty on the latter figure may then dominate and practically set the accuracy on the LFI estimate of $T^{(b)}$; therefore, even a poor knowledge of this contribution (e.g., with an accuracy of $\sim 30\%$) allow to reach a $\simeq 1\%$ level of accuracy in the measurement of $T^{(b)}$ (Burigana et al. 2000c).

So far no systematic effect has been included in the simulations. One of the main goals of the PLANCK mission is to limit the contamination arising from systematics at few μK level. However, systematics affecting the spacecraft pointing and rotation, which are not expected to significantly degrade the sky temperature estimation, may in principle turn out to be harmful when reconstructing the beam shape. To investigate this possibility we have extended our simulation to include these effects.

² We want to stress that the calibration of the TOD is not needed in order to reconstruct the other beam parameters.

3.1.1. Pointing uncertainty

A potential problem for in-flight beam reconstruction is posed by the telescope pointing uncertainty, i.e. the limited accuracy in determining the spacecraft’s effective spin axis. However, it is a PLANCK requirement that such an uncertainty be less than $1'$. This is why, to simulate this effect we introduce a pointing uncertainty drawn from uniform distribution of values between 0 and 1. Since the spin axis direction is not expected to significantly change within the same scan, the uncertainties only arising when the spacecraft is repointed, we keep the perturbation constant along the scan.

The impact of pointing uncertainty in the elliptical beam parameter recovery for the first transit of Jupiter and Saturn is also shown in Table 2. Clearly, the higher signal to noise ratio in case of Jupiter makes the results more sensitive to this kind of systematics. This is evident from the larger degradation of the beam parameter recovery. Although the degradations in the recovered parameters are well above the corresponding quoted statistical errors, we do not find a particularly critical effect on the various parameters, except for the parameter $r-1$, affected by an error of 10% by using Jupiter, for the adopted level of pointing uncertainty. On the other hand, the analysis of the χ^2/DOF ($\simeq 1.3$) clearly flags this problem. In this circumstance, it may be then particularly safe to take advantage of the Saturn transits, that, although intrinsically noisier, are significantly less affected by this kind of systematics. We can then exploit the Jupiter transits to check the fit results where the signal to noise ratio from Saturn transits decreases.

The reported values of χ^2/DOF can be understood on the basis of simple considerations. The derivative of a Gaussian response, $J = \exp[-(\theta/\sigma)^2/2]$, with respect to the angle θ from the beam center at $\theta \sim \sigma$ is given by $dJ/J \sim -d\theta/\sigma$; for Jupiter (Saturn), the signal at $\theta \sim \sigma$ is ~ 22 mK (~ 5 mK) for a beam with a FWHM $\sim 33'$. Then, a pointing error $d\theta \sim 1'$ about $\theta \sim \sigma$ implies a signal change of ~ 1.6 mK (~ 0.35 mK). Let’s assume such value of error in a squared region about the beam center with a 2σ side, containing ~ 32 samplings in the current simulations. The fit uses $\sim 10^4$ samplings with a white noise sensitivity of ~ 0.17 mK. We find then a χ^2/DOF of $(10^4 \times 0.17^2 + 32 \times 1.6^2)/(10^4 \times 0.17^2) \sim 1.3$ for Jupiter (and analogously ~ 1.01 for Saturn), in good agreement with the values reported in Table 2.

3.1.2. Spacecraft rotation

We have also verified the effect the spacecraft rotation during single sample integration. Strictly speaking, the signal inside each sampling time changes according to the beam response. We can take this effect into account by oversampling and then averaging the simulated data inside each sampling time and by equivalently implementing in the fit

procedure the recovery of the intrinsic (i.e. non affected by rotation) optical beam parameter. We have here implemented the impact of the satellite rotation only in the data flow generation, in order to estimate the error introduced in the beam parameter recovery by a simple fit procedure that does not take into account this effect. The results are again reported in Table 2 for the first transit of Jupiter and Saturn in the case of an elliptical beam. As expected, the effect on beam position and inclination is negligible. Since in the present test the minor axis is taken along the scan circle direction, the beam is reconstructed with a smaller ellipticity and a larger FWHM with respect to the input values, with no indication of a worsening of the χ^2/DOF . Clearly, in the general case, the final effect will depend on a combination of beam ellipticity and inclination with respect to the sky scan direction. The beam parameters recovered by neglecting the spacecraft spinning within the sampling time in the fit procedure may also be seen as characterizing the “effective” properties of the beam in presence of spacecraft rotation. Again, the “effective” values of σ reported in Table 2 are in agreement with simple analytical considerations. In fact, the effective resolution which takes into account the intrinsic beam optical resolution and the beam smearing introduced by the satellite rotation is well approximated by $\sigma_{eff} = \sqrt{\sigma^2 + \theta_s^2/12}$ where θ_s is the angle ($\simeq 5'$ for the present simulations) in the sky described by the beam axis during the sampling time.

3.2. Recovery of the main beam shape

We consider here the capability to reconstruct in flight the detailed shape of the main beam by using Jupiter transits. We apply our method to a beam @ 30 GHz simulated through the GRASP8 code for the Alcatel case1 telescope configuration (see Fig. 3), an aplanatic solution like those suggested by Mandolesi et al. 2000b in order to minimize the coma distortion and render the main beam shapes close to ellipses. In this case we adopt a simple scanning strategy with $\alpha = 80^\circ$, the same scan angle considered in the Alcatel case1 design, shift the spin axis of $2.5'$ every hour and oversample each scan circle every $\simeq 11'$ (i.e. roughly 3 points per FWHM @ 30GHz).

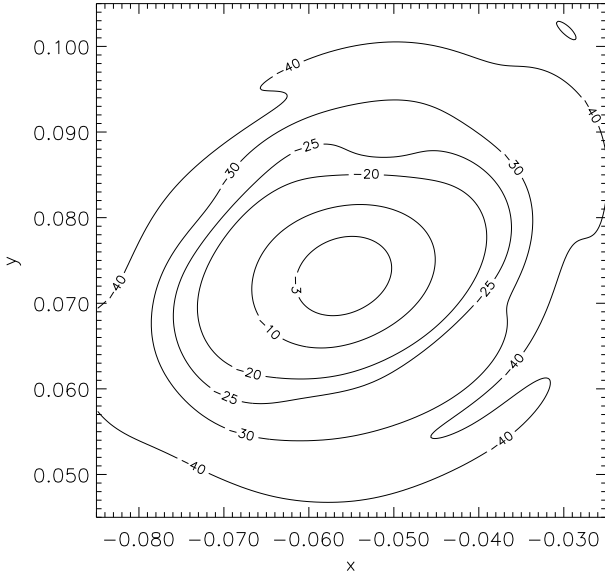
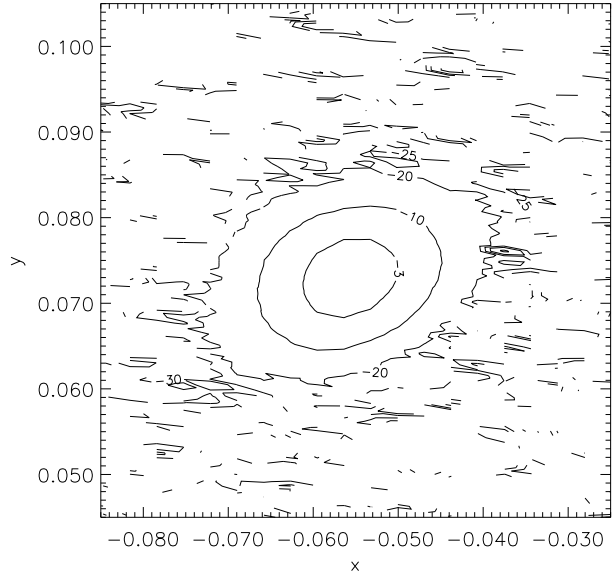
By inverting Eq. (1) we derive the beam pattern shape. Fig. 4 show the results obtained @ 30 GHz by considering the sensitivity of the two radiometers coupled to a single beam and a single Jupiter transit: the main beam shape can be directly recovered down to $\simeq -20$ dB with good accuracy. The result clearly improves by adding three Jupiter transits and taking into account the possibility of averaging the recovered shapes of the two equivalent beams at the same frequency, as shown in Fig. 5.

By fitting the TOD with the method described in Sect. 3.1 we can derive the beam parameters under the assumption of a circular or bivariate Gaussian shape. The results are reported in Table 2. We show also respectively

Table 1. Input parameters of symmetric and elliptical beam for the considered planet transits.

Input values								
Event	ϵ (deg)		σ (arcmin)	r		r_k [‡] (mK)	$x_T^* \cdot 10^2$ —	$y_T^* \cdot 10^2$ —
	<i>circ.</i>	<i>ellipt.</i>		<i>circ.</i>	<i>ellipt.</i>			
Jupiter (I)	—	0	14.01381	1	1.3	35.8297	-5.76035	7.91971
Jupiter (II)						35.4743		
Saturn (I)						7.8543		
Saturn (II)						7.8229		

[‡] The value r_k depends on the distance between the spacecraft and the planet which slightly varies between different pointing events.

**Fig. 3.** Contour plot (in dB) of one of the two beams @ 30 GHz as simulated through the GRASP8 code for the Alcatel case1 telescope configuration.**Fig. 4.** Reconstruction of the beam of Fig. 3 by using a single Jupiter transit and the sensitivity of the two radiometers coupled to the beam.

in Figs. 6 and 7 the comparison between the input beam shape and the recovered one for the case of circular and bivariate Gaussian approximation. As evident, the bivariate approximation represents a significant improvement with respect to the circular one, as indicated by the value χ^2/DOF , respectively 1.232 and 8.094. The agreement between the bivariate approximation and the simulated beam results quite good down to $\simeq -25$ dB. At lower response levels the Gaussian behavior begins to significantly underestimate the beam response, even in the bivariate approximation.

Finally, we simulate Jupiter transits as seen by an elliptical beam with the same parameters derived from the fit of the simulated beam, but in the case of the current simple baseline scanning strategy defined by $\alpha = 85^\circ$, spin axis shift of $2.5'$ every hour and by approximately 3 samplings per FWHM (i.e. one point every $\simeq 11'$ along a scan circle @ 30 GHz). As expected, the beam parameters are

recovered with an accuracy essentially unchanged with respect to the results of Sect. 3.1 (see the last row of Table 2), in spite of the less regular grid in the $x_T - y_T$ plane, less refined (by a factor $\simeq 4$) along the scan direction than along that of the spin axis repointing.

3.3. Circular versus elliptical approximation of the beam shape

A crucial point for CMB anisotropy experiments is to estimate the impact of the quality of the main beam reconstruction on the data analysis and, ultimately, on the sky maps that can be obtained and on the related science. An accurate discussion of this problem is not the aim of this work. Nevertheless, we want address here this argument. By including also the Galaxy emission, only at low Galactic latitudes and at the lowest LFI frequencies the impact of elliptical main beam distortions significantly increases

Table 2. Recovery of the beam parameters from the considered planet transits in presence of pure white noise and taking also into account two kinds of systematical effects. Circular, elliptical and simulated beams as well as different values of the boresight angle α are considered.

Event	ϵ (deg)	σ (arcmin)	r –	r_k (mK)	$x_T^* \cdot 10^2$ –	$y_T^* \cdot 10^2$ –	χ^2/DOF –
<i>Circular beam</i>							
Jupiter (I)	–	14.0071 ± 0.0089	1.0039 ± 0.0012	35.877 ± 0.032	–5.7602 ± 0.0004	7.9192 ± 0.0004	0.994
Jupiter (II)	–	14.0126 ± 0.0092	1.0010 ± 0.0013	35.486 ± 0.033	–5.7603 ± 0.0004	7.9200 ± 0.0004	0.997
Saturn (I)	–	13.996 ± 0.042	1.0067 ± 0.0061	7.839 ± 0.033	–5.7659 ± 0.0020	7.9204 ± 0.0015	0.998
Saturn (II)	–	14.034 ± 0.042	1.0078 ± 0.0061	7.797 ± 0.033	–5.7637 ± 0.0020	7.9209 ± 0.0015	1.007
<i>Elliptical beam</i>							
Jupiter (I)	–0.0059 ± 0.0024	14.0095 ± 0.0088	1.3023 ± 0.0016	35.876 ± 0.032	–5.7602 ± 0.0004	7.9193 ± 0.0003	0.995
Jupiter (II)	0.0011 ± 0.0025	14.0102 ± 0.0092	1.2993 ± 0.0017	35.491 ± 0.033	–5.7603 ± 0.0004	7.9199 ± 0.0003	0.997
Saturn (I)	–0.007 ± 0.011	14.004 ± 0.042	1.3055 ± 0.0078	7.837 ± 0.033	–5.7661 ± 0.0020	7.9199 ± 0.0015	0.999
Saturn (II)	0.009 ± 0.011	14.041 ± 0.042	1.3073 ± 0.0078	7.796 ± 0.033	–5.7645 ± 0.0020	7.9207 ± 0.0015	1.007
<i>Elliptical beam: effect of 1' pointing error</i>							
Jupiter (I)	0.0288 ± 0.0025	13.7895 ± 0.0089	1.3424 ± 0.0017	35.884 ± 0.032	–5.7576 ± 0.0004	7.9227 ± 0.0003	1.329
Saturn (I)	–0.005 ± 0.011	14.004 ± 0.043	1.3060 ± 0.0078	7.819 ± 0.033	–5.7589 ± 0.0020	7.9118 ± 0.0015	1.011
<i>Elliptical beam: effect of neglecting spacecraft motion</i>							
Jupiter (I)	0.00367 ± 0.0025	14.0697 ± 0.0089	1.2904 ± 0.0016	35.584 ± 0.032	–5.7602 ± 0.0004	7.9198 ± 0.0003	0.999
Saturn (I)	–0.007 ± 0.012	14.053 ± 0.043	1.2964 ± 0.0078	7.782 ± 0.033	–5.7661 ± 0.0020	7.9200 ± 0.0015	0.999
<i>Alcatel case1 beam: fit with circular beam – realistic simple scanning strategy, $\alpha = 80^\circ$</i>							
Jupiter (I)	–	14.9583 ± 0.0089	–	31.106 ± 0.026	–5.5751 ± 0.0003	7.2991 ± 0.0004	8.094
<i>Alcatel case1 beam: fit with elliptical beam – realistic simple scanning strategy, $\alpha = 80^\circ$</i>							
Jupiter (I)	20.97 ± 0.11	15.0102 ± 0.0087	1.3602 ± 0.0016	31.360 ± 0.026	–5.5756 ± 0.0003	7.3001 ± 0.0004	1.232
<i>Above elliptical beam: fit with elliptical beam – baseline simple scanning strategy, $\alpha = 85^\circ$</i>							
Jupiter (I)	21.01 ± 0.10	15.0209 ± 0.0083	1.3590 ± 0.0015	32.241 ± 0.025	–5.5792 ± 0.0003	7.2794 ± 0.0004	0.997

(by a factor $\simeq 3$) with respect to the case of a pure CMB fluctuation sky (Burigana et al. 1998) whereas only very small effects are added by the combined effect of realistic main beam distortions and extragalactic source fluctuations (Burigana et al. 2000a). In addition, the main beam distortion impact moderately increases with the FWHM (Burigana et al. 1998) for the LFI resolution range. Therefore, we will consider here for simplicity a pure CMB fluctuation sky in a reference case of a standard Λ CDM model approximately COBE/DMR normalized and consider for the present analysis the 30 GHz channel. In Fig. 8 we report the difference between the signals obtained by convolving the sky with the bivariate main beam and with the circular main beam by assuming in each case the cor-

responding set of parameters that fits the simulated beam (see Table 2). The rms of the temperature differences is $\simeq 4.1\mu\text{K}$. A similar comparison but between the circular and the simulated beam (see Fig. 9) gives a very similar rms value, $\simeq 4.7\mu\text{K}$. This suggests that the ellipticity is the most relevant feature of the main beam shape. In fact, the comparison between the convolutions with the bivariate Gaussian beam and the simulated one (see Fig. 10) gives a rms temperature difference of $\simeq 1.7\mu\text{K}$, a factor $\simeq 3$ smaller than that obtained by approximating the beam with a symmetric Gaussian shape.

Of course, when the PLANCK optical design will be settled and the main beam patterns computed through optical simulation codes it would be possible to search for

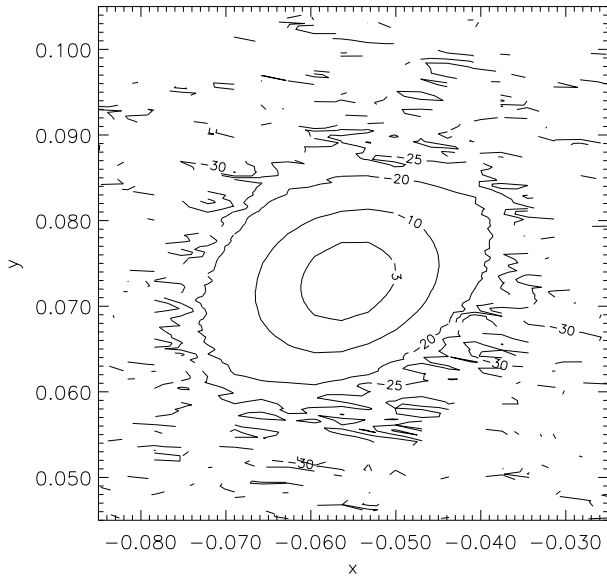


Fig. 5. Reconstruction of the beam of Fig. 3 by using three Jupiter transits and two radiometers per beam and by taking advantage from the identical optical properties of the two 30 GHz beams.

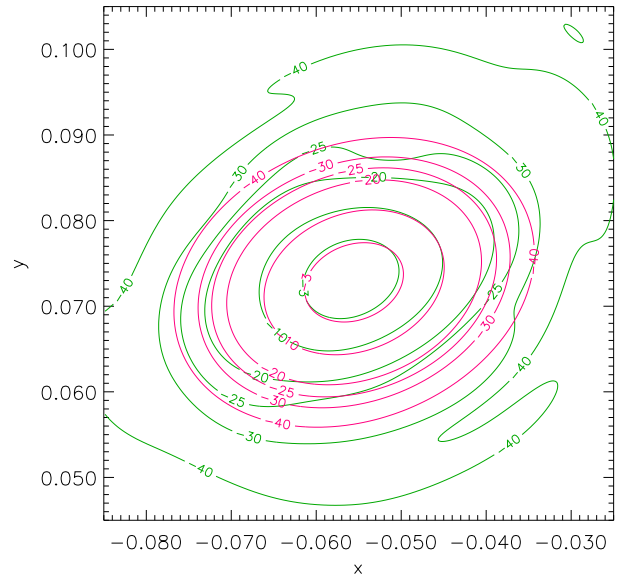


Fig. 7. Comparison between the simulated beam and its approximation in terms of elliptical Gaussian beam (see also Table 2).

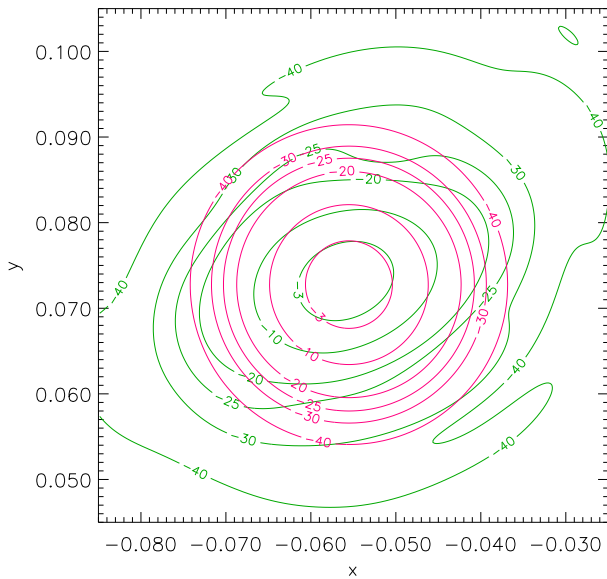


Fig. 6. Comparison between the simulated beam and its approximation in terms of circular Gaussian beam (see also Table 2).

analytical descriptions of main beam shapes that might improve the bivariate Gaussian approximation. Anyway, we have proved here that this representation allow to reach the $\simeq \mu\text{K}$ accuracy level in the treatment of PLANCK-LFI TOD's.

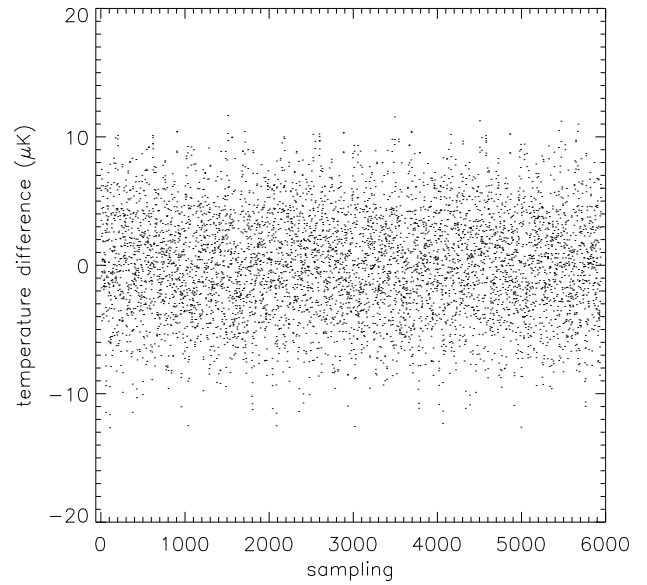


Fig. 8. Difference between the TOD from the elliptical beam and the circular beam that fit the input beam for three scan circles.

4. Straylight from Moon, Earth and Sun

By using the same method described in Sect. 2 and the full antenna pattern shown in Fig. 1 (de Maagt et al. 1998), we are able to quantify the impact of the internal Solar System objects to the PLANCK-LFI observations. The Moon, the Earth and the Sun are the only internal bodies that

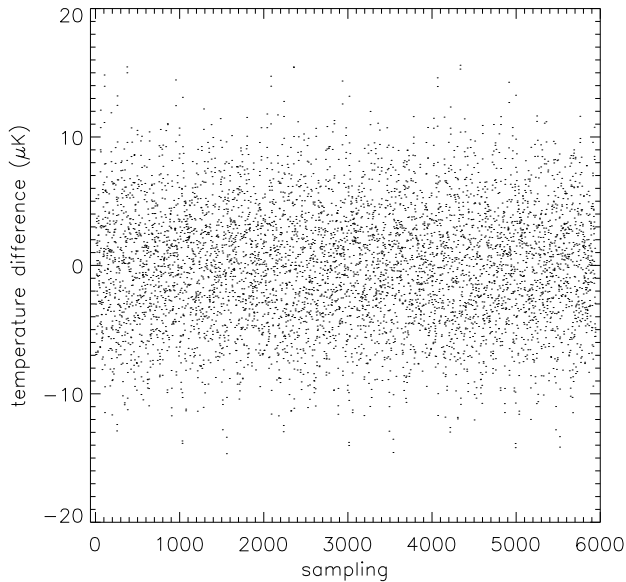


Fig. 9. Difference between the TOD from the circular beam and the simulated beam for the same three scan circles of Fig. 8.

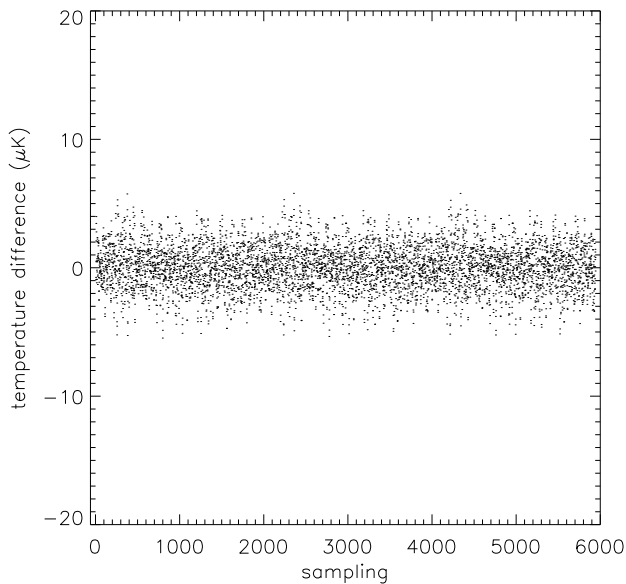


Fig. 10. Difference between the TOD from the elliptical beam and the simulated beam for the same three scan circles of Fig. 8. By comparing this figure with Fig. 9 the improvement with respect to the circular approximation of the main beam is evident.

may introduce appreciable straylight contamination. The solid angle of these objects, although not negligible, is very small compared to the angular scale for which significant variations of the far pattern response occur; this makes the use of Eq. (2) accurate enough for the present purposes.

Of course, the level of straylight contamination from these bodies depends also on the effective scanning strategy. We studied a Lissajous orbit around L2 for the PLANCK surveyor (Bersanelli et al. 1996) by considering *case i*) the simple scanning strategy with the spin axis always parallel to the Sun–spacecraft direction and *case ii*) a precession motion of the satellite spin axis like that discussed in Sect. 2.1. [For this straylight analysis we assume $\alpha = 80^\circ$, the value adopted in the optical computation by de Maagt et al. 1998].

By coadding the TOD computed as described in Sect. 2 we have produced nearly full sky maps of averaged straylight contamination (see Burigana et al. 2000b for further details). [We adopt here the HEALPix pixelisation by Górski et al. 1998]. We find that in any case this effect is very small, with the maximum contamination level always below $0.15 \mu\text{K}$. Although small, this effect has to be considered with caution. In fact, this straylight contamination is produced by the very low response antenna in the “antispillover” region, where an accurate antenna response measurement is extremely difficult.

5. Discussion and conclusions

We implemented the PLANCK flight simulator (Burigana et al. 1997, 1998, Maino et al. 1999) to properly discuss the impact of the Solar System main bodies on the PLANCK observations. In particular, we focused on the problem of the in-flight reconstruction of the main beam of the PLANCK-LFI antenna patterns. To do so, we simulate in details the transits of Jupiter and Saturn in the field of view of the PLANCK-LFI, 30 GHz beam. The method can be easily extended to the other PLANCK channels. Our analysis shows that, using Jupiter, we can recover in flight the main beam response down to $\sim -(25 \div 32.5)$ dB, where the signal to noise ratio approaches unity.

Both symmetric and non symmetric beams have been considered; in the latter case we assumed a simple elliptical shape, as suggested by recent optical simulations (Mandolesi et al. 2000b), but the method can be generalized to more refined parametrizations.

We have demonstrated that the key parameters of the main beam (resolution, ellipticity, position and inclination on the plane of PLANCK field of view) can be simultaneously recovered with high precision by fitting the planet transit signal. Of course, the larger signal to noise ratio of Jupiter (compared to that of Saturn) translates in a better parameter recovery, by a factor $3 \div 5$.

After having considered the idealized case of pure white noise, we discussed possible degradations to the main beam reconstruction introduced by the effects of spacecraft pointing relevant in this context. Spacecraft rotation does not affect significantly the quality of the reconstruction; on the contrary, by neglecting the spacecraft rotation in the fit procedure we derive the effective beam parameters including rotation smearing effect. The most

relevant source of contamination is represented by the spin axis pointing uncertainty which can degrade the recovery of the beam ellipticity parameter $r - 1$ by $\simeq 10\%$ in the case of $1'$ pointing error when Jupiter is used. In these circumstance, clearly recognizable through the increase of the χ^2/DOF , we find very advantageous to consider Saturn, that produce information less sensitive to this kind of systematics.

To complete the analysis, we considered also the full recovery of a simulated beam shape for an aplanatic configuration of the optical design recently studied by Alcatel. The beam shape can be reconstructed with good accuracy and resolution down to -25 dB. Of course, somewhat lower response levels at larger angles from the beam centre can be measured in flight by relaxing the requirement of recovering the beam shape with the same resolution necessary to accurately describe the more central regions of the main beam.

We addressed the study of the impact of the quality of the main beam reconstruction on the treatment of LFI TOD's. We shown that a bivariate Gaussian approximation represents a significant improvement with respect to a symmetric representation. A rms difference of $\simeq 1.7\mu\text{K}$ is found between the TOD obtained by convolving a CMB fluctuation sky with a simulated beam or its bivariate Gaussian approximation as derived by the in-flight reconstruction, a result better by a factor three with respect to the case of the symmetric approximation.

The possibility to combine a very accurate in-flight calibration by using the CMB dipole (Bersanelli et al. 1997) and the good accuracy in the recovery of the maximum signal (the parameter r_k in Table 2) at the planet transit, offers a good chance of measuring the intrinsic planet temperatures at millimetric wavelengths with an accuracy at % level, the main source of error being the uncertainty on the integrated antenna pattern response. This represents an interesting byproduct of PLANCK observations.

Finally, we have shown that the effect of Sun, Earth and Moon in the far sidelobes produces sub- μK effects independent of the details of the scanning strategy.

To summarize, at least at 30 GHz, observation of external planets offers an accurate, robust and simple method to reconstruct in flight the main beam properties under very general conditions.

Acknowledgements. It is a pleasure to thank C.R. Butler, B. Cappellini, G. Cremonese, D. Maino, F. Pasian and F. Villa for useful discussions on PLANCK design and performances and on planet emission properties. We gratefully acknowledge K.M. Górski and all the people involved in the realization of the tools of HEALPix pixelisation, employed here in the straylight analysis. We gratefully thank P. de Maagt and J. Tauber for having provided us with their optical simulation results and F. Villa for having computed with the GRASP8 code the main beam pattern

LFI27 for the Alcatel case1 configuration with the high resolution grid adopted in this study.

References

- Bersanelli M., et al., 1996, ESA, COBRAS/SAMBA Report on the Phase A Study, D/SCI(96)3
- Bersanelli M., et al., 1997, A&AS, 121, 393
- Burigana C., et al., 1997, Int. Rep. TeSRE/CNR 198/1997, November 1997, astro-ph/9906360
- Burigana C., et al., 1998, A&AS, 130, 551
- Burigana C., et al., 2000a, Astro. Lett. Comm., 37, 253
- Burigana C., et al., 2000b, Int. Rep. TeSRE/CNR 272/2000, April 2000
- Burigana C., et al., 2000c, Int. Rep. TeSRE/CNR 273/2000, April 2000
- De Maagt P., Polegre A.M., Crone G., 1998, PLANCK – Straylight Evaluation of the Carrier Configuration, Technical Report ESA, PT-TN-05967, 1/0
- Górski K.M., Hivon E., Wandelt B.D., 1998, to appear in “Proceedings of the MPA/ESO Conference on Evolution of Large-Scale Structure: from Recombination to Garching”, Banday A.J et al. (Eds.), astro-ph/9812350
- Maino D., et al., 1999, A&AS, 140, 1
- Mandolesi N., et al., 1998, PLANCK Low Frequency Instrument, A Proposal Submitted to the ESA
- Mandolesi N., et al., 2000a, A&AS, 145, 323
- Mandolesi N., et al., 2000b, Astro. Lett. Comm., 37, 151
- Puget J.L., et al., 1998, High Frequency Instrument for the PLANCK Mission, A Proposal Submitted to the ESA
- Seiffert M., et al., 1997, Rev. Sci. Instrum., submitted